Asian Journal of Chemistry; Vol. 35, No. 7 (2023), 1632-1644

ASIAN JOURNAL OF CHEMISTRY

https://doi.org/10.14233/ajchem.2023.27926

Synthesis, Characterization, Biological Activity and Molecular Docking Studies of Phthalic Acid based Macrocyclic Transition Metal Complexes

RAJRANI GULIA[1], VIKAS SANGWAN[2], ANSHUL SINGH[1,*], SONAXI KHARB[1] and RITU SOLANKI[3]

[1]Department of Chemistry, Baba Mastnath University, Rohtak-124021, India
[2]Department of Chemistry, R.P.S. Degree College, Mahendergarh-123029, India
[3]Department of Biochemistry, Maharshi Dayanand University, Rohtak-124001, India

*Corresponding author: E-mail: anshul9008@gmail.com

Received: 23 April 2023; *Accepted*: 25 May 2023; *Published online*: 6 July 2023; AJC-21285

A novel series of macrocyclic complexes of $[M(L)Cl_2]$ (M = Co(II), Ni(II) and Cu(II), L = macrocyclic ligand) were synthesized by template condensation method using 3,4-diaminotoluene and phthalic acid in the presence of divalent transition metal ions *e.g.*, Co(II), Ni(II) and Cu(II) in their chloride form. These synthesized metal complexes were fully characterized by spectroscopic techniques, namely UV-Visible, IR, ESR and ESI-MS. Their thermal behaviour was determined by TGA and DTA. Further these macrocyclic complexes were screened for antimicrobial activity against bacterial species (*Staphylococcus aureus*, *Bacillus subtilis*, *Pseudomonas aeruginosa* and *Escherichia coli*) and fungi (*Aspergillus niger* and *Candida albicans*) and then compared against standard drug streptomycin and itraconazole, respectively. In addition to these the antioxidant activity of the macrocyclic complexes were also investigated through scavenging effect on the DPPH radicals. Finally, the biological potency of synthesized compounds was evaluated using Auto Dock Vina. All the synthesized macrocyclic complexes were found to be potent against bacterial and fungal species, which suggest their potential application as antibacterial and antifungal agents.

Keywords: Macrocyclic complexes, Template condensation, Antimicrobial, Tetra-aza macrocyclic, Molecular docking.

INTRODUCTION

Recent years have witnessed an immense deal of interest in the vicinity of synthesis of transition metal complexes with macrocyclic ligands. In past few years, the macrocyclic ligands have acquired great interest of chemists due to their mind-boggling chemical and biological properties. Various macrocyclic Schiff bases are essential in the coordination chemistry owing to the fact they can selectively chelate certain metal ions relying at the wide variety, type and position of their donors [1-6]. The layout and synthesis of novel medicines that beautify their assessment and the simultaneous advances in relevant technology contributed to the recent trends on this vicinty [7]. Owing to these chemical properties among the chemistry of transition metals, several macrocyclic complexes have been found with high biological relevance. In spite of having these properties, these metal macrocyclic complexes serve as biochemical complex for related metalloenzymes. However, in addition they also provide insights into the biomimic models [8,9].

These macrocyclic complexes of transition metal ions had been demonstrated to be a precious form of the auxiliary ligands for several metallomolecules such as porphyrins, corrins by the change within the size of ring and the donor atom in the macrocyclic ligand [10]. Owing to their unique properties in the better understanding of the molecular processes of biochemical, clinical application, analytical, contrast agents in magnetic resonance imaging, antimicrobial agents [11] and catalysis [12] several polyaza macrocyclic complexes have been synthesized [13-19]. The family of metal complexes with the aza macrocyclic ligands has remained a focal point of clinical interest for past a long time. Cyclen and cyclam are the tetraaza macrocyclic complexes which strongly bind with broad array of metallic ions with frequent applications in medicinal world [20-26]. These complexes with metal ions have been studied as antimalarial, antileishmanial, anticancer and anti-schistomal agents

This is an open access journal, and articles are distributed under the terms of the Attribution 4.0 International (CC BY 4.0) License. This license lets others distribute, remix, tweak, and build upon your work, even commercially, as long as they credit the author for the original creation. You must give appropriate credit, provide a link to the license, and indicate if changes were made.

[27]. In connection with the preceding investigations, on coordinating properties of the tetraaza macrocycles and as a way to isolate novel metal macrocyclic complexes with potential antimicrobial and antioxidant properties, we have studied the synthesis, spectroscopic and biochemical components of macrocyclic complexes of cobalt(II), nickel(II) and copper(II) derived from phthalic acid and 3,4-diaminotoluene.

EXPERIMENTAL

The divalent metal salts used for synthesis were purchased from E. Merck and Ranbaxy, India. Phthalic acid and 3,4-diaminotoluene (4-methyl-*o*-phenylene diamine) (DAT) were procured from Sigma-Aldrich. All the solvents like methanol, dimethyformamide (DMF), diethyl ether and DMSO were of reagent grade and used without further purification.

Synthesis of metal complexes: For the synthesis of macrocyclic metal complexes the molar ratios of 2:1:2 were used to carry out reaction. The progression involves refluxing of methanolic solution (50 mL) of 3,4-diaminotoluene (10 mmol) and methanolic solution (20 mL) of divalent metallic salt, respectively (5 mmol) for 30 min. After 30 min, 20 mL of methanolic solution of phthalic acid (10 mmol) was added to the above refluxed mixture. Subsequently, refluxing was continued for 8-10 h. The mixture was set aside at room temperature in desiccators. The slight colour change provided an indication for the complexation. These coloured precipitates of complexes were then filtered and washed with solvents (methanol and acetone) and then dried (**Scheme-I**). The synthesized metal complexes were found to be soluble in methanol, isopropyl alcohol, acetone, DMF and DMSO.

[Co($C_{30}H_{24}N_4O_4Cl_2$)] (DP1): Yield: ~69%, light purple colour, *m.w.*: 632.93, molar conductivity (21 Ω^{-1} mol^{-1} cm^2), μ_{eff} (B.M.): 3.8, UV-visible [DMSO, λ (nm)]: ~320, ~270 and ~210 nm.

[Ni($C_{30}H_{24}N_4O_4Cl_2$)] (DP2): Yield: ~65%, light green colour, *m.w.*: 632.69, molar conductivity (19 Ω^{-1} mol^{-1} cm^2), μ_{eff} (B.M.): 2.83, UV-visible [DMSO, λ (nm)]: ~550, ~280 and ~230 nm.

[Cu($C_{30}H_{24}N_4O_4Cl_2$)] (DP3): Yield: ~78 %, black colour, *m.w.*: 637.54; molar conductivity (11 Ω^{-1} mol^{-1} cm^2), μ_{eff} (B.M.): 1.73, UV-visible [DMSO, λ (nm)]: ~560, ~280 and ~230 nm.

Analytical data and physical properties: Assistance of digital conductivity meter (HPG System, G-3001) was taken for determining the molar conductance values of complexes. A Cary 14 spectrophotometer was used for the recording of electronic spectra in DMSO. The IR spectra were conducted by using KBr pellets on a Fourier-Transform IR spectrophotometer (Agilent Technologies) in the range of 4000-400 cm^{-1}. The determination of melting points was carried out on an electrical melting point instrument and are uncorrected. EPR characterization of the sample was performed on an ESR, Varian, USA at room temperatures. The powder X-ray diffraction was recorded on Empyrean X-ray diffractometer. The TGA analysis was conducted on the Thermogravimetric analyzer (Hitachi STA 650) TGA instruments.

Biological assays: The agar well diffusion method has been used for evaluating *in vitro* antimicrobial activity of the synthesized macrocyclic complexes. For these evaluations two Gram-positive bacteria (*Staphylococcus aureus* and *Bacillus subtilis*) and two Gram-negative bacteria (*Escherichia coli* and *Pseudomonas aeruginosa*) were selected. The synthsized complexes were also assessed for antifungal activity two fungi (*Aspergillus niger* and *Candida albicans*).

***In vitro* antibacterial activity:** The antibacterial efficacy of the synthesized macrocyclic complexes has been investigated through Agar well plate diffusion method. For this 11.5 g of Muller Hinton powder was used in 300 mL of water to prepare a solution and then sterilized by the autoclave at 121 ºC for 20 min. The pH of the medium is specifically maintained around

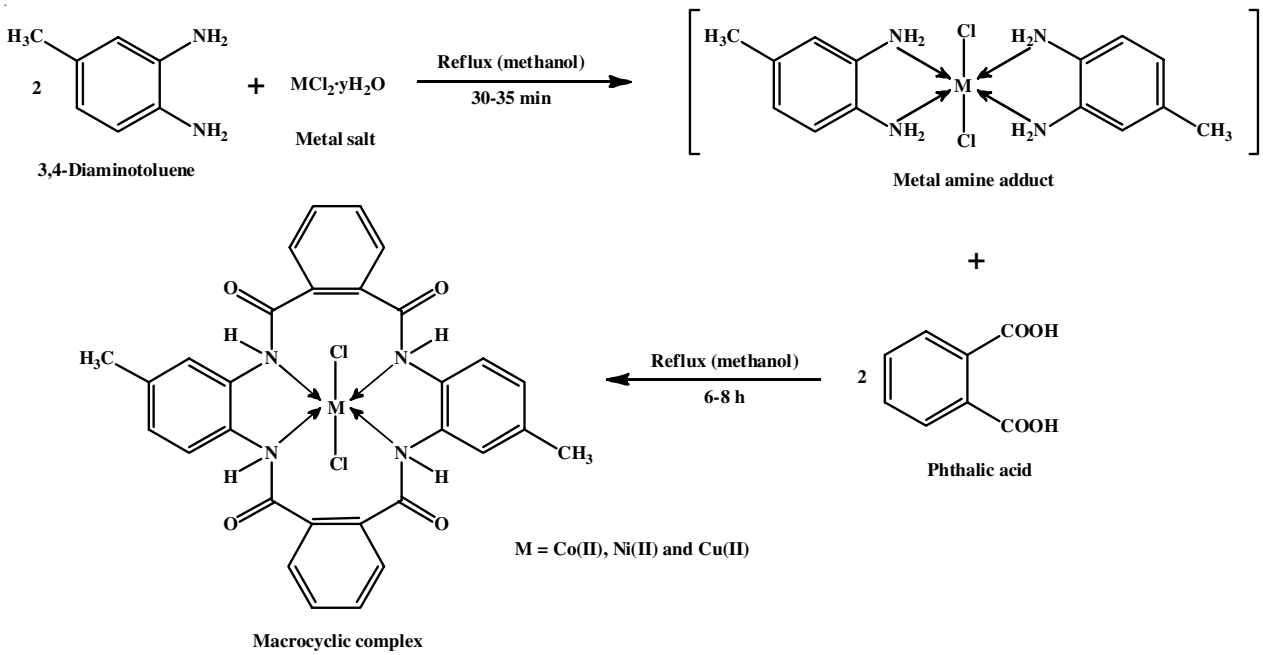

Scheme-I: Schematic representation of synthesizing macrocyclic complexes of transition metal ions

the physiological pH of 7.4. After cooling, approximately 25-30 mL of medium was added aseptically to the sterilized 100 mm × 15 mm petri dishes. The complexes were dissolved in DMSO and stock solutions (2.5 mg/mL, 5.0 mg/mL and 7.5 mg/mL) were prepared and 50 µL of these were used in each of the well. Agar plates were prepared for the selected antibacterial strains. The petri plates incorporated selected bacterial strains were incubated at 37 ºC for 24 h. Further, the bacterial activity of all the three complexes were observed and compared with the standard drug streptomycin [28,29].

***In vitro* antifungal activity:** The antifungal efficacy of macrocyclic complexes was assessed using agar well plate diffusion method. An Agar medium was prepared by dissolving 19.5 g of Saboraud dextrose agar powder in 300 mL of water, which was then sterilized in autoclave at 121 ºC for 20 min. The pH of about 7.2 was specifically maintained for the medium. After cooling, approximately 30 mL of medium was added aseptically to the sterilized 100 mm × 15 mm Petri dishes [30,31].

The microorganisms to be tested were spread evenly on the plates using a sterile swab and then 6 mm diameter wells were formed using the sterile well borer, a volume of 50 µL macrocyclic complexes with the concentrations of 2.5 mg/mL, 5.0 mg/mL and 7.5 mg/mL were added into these wells. The Petri plates incorporating Gram-positive and Gram-negative bacterial culture were incubated at 37 ºC for 24 h while fungal culture petri plates were incubated at 28 ºC for 48 h to provide optimal conditions for the growth of the bacteria and fungi, respectively. The average diameter of the inhibition zone around 6 mm wells has been calculated to the nearest 0.5 mm resolution with the ruler after incubation. The mean and standard deviations of macrocyclic complexes were based on triplicates using DMSO as solvent. All these complexes were evaluated against the standard drug itraconazole [28].

Antioxidant activity: The radical scavenging activity of the complexes has been evaluated through DPPH (2,2Diphenyl-1-picrylhydrazyl) assay and then compared with that of the standard.

DPPH assay: The DPPH assay [32] was evaluated for the determination of free radical scavenging activities of the synthesized macrocyclic complexes. For this objective, various concentrations (3, 6, 9, 12, 15 and 18 µg/mL) of the complexes and the standard (ascorbic acid) have been prepared. Ascorbic acid was diluted to 3 mL with ethanol and 1 mL of ethanolic DPPH solution (2,2Diphenyl-1-picrylhydrazyl) of 0.1 mM was added to the complexes. These complexes were incubated in the dark for around 0.5 h around 30 ºC. The reduction in the solution of DPPH absorbance after the regular addition of an antioxidant was measured at 517 nm against the blank complex. Ascorbic acid (10 mg/mL DMSO) has been used as a reference. DPPH is a free radical with that of purple red colour; it becomes yellow colour after scavenging. Antioxidant reacts to DPPH solution and further it reduced to DPPH-H and thence absorbance reduces. DPPH free radicals of several concentrations of the complexes and the standard solution were measured by using the following eqn.:

$$\text{Radical scavenging capability } (\%) = \frac{A_{control} - A_{sample}}{A_{control}} \times 100$$

where $A_{control}$ is the absorbance of DPPH radical and ethanol; A_{sample} is the absorbance of the DPPH radical and macrocyclic complex.

Molecular docking study: Molecular docking assays were performed using AutoDock Vina to understand the different methods of interactions of proteins from different origins with metal-coordinated macrocyclic ligands (DP1, DP2 and DP3). These macrocyclic complexes were docked with various receptor protein targets, comprising *E. coli* (3T88), *P. aeruginosa* (2W7Q), *B. subtilis* (5H67), *S. aureus* (2DHN), *C. albicans* (3DRA) and *A. niger* (6IGY). The target proteins were optimized by removing the water molecule as they may interfere with the protein-ligand interaction, adding polar hydrogens as these might get involved in hydrogen bonding. The output of the prepared protein was written in PDBQT format after the addition of Kollmann charges.

The structure of ligands was then drawn using Avogadro software [33,34] and saved in MOL2 format after optimization in three-dimensional structure through UFF (universal force-field) as MOL2 format is compatible with AutoDock Vina [35, 36]. The algorithm was set to the steepest descent during geometry optimization and four steps per update. The ligands were loaded to AutoDock GUI with the addition of Gasteiger charges, the merging of non-polar hydrogens, default identification of rotatable bonds and finally converting the ligands to PDBQT format.

Binding modes of cobalt (DP1), nickel (DP2) and copper (DP3) complexes with receptors were identified using the AutoDock Vina software program. Lamarckian Genetic Algorithm was used to resolve the optimized conformation [37]. PDBQT files of target protein and ligands were uploaded with the grid spacing of 0.503 Å and grid center coordinates were set at X, Y and Z axes at 40 × 40 × 40. The number of exhaustiveness was set to 8. All possible conformations were derived through the program and conformation with the least energy binding was selected. Output log files were visualized in Chimera [38] and Discovery Studio Visualiser.

RESULTS AND DISCUSSION

The tetraaza macrocyclic complexes $[Co(C_{30}H_{24}N_4O_4Cl_2)]$, $[Ni(C_{30}H_{24}N_4O_4Cl_2)]$ and $[Cu(C_{30}H_{24}N_4O_4Cl_2)]$ were derived from phthalic acid and 3,4-diaminotoluene (4-methyl-*o*-phenylene diamine) by the route of template method (**Scheme-I**). All the synthesized tetraaza macrocyclic complexes are of coloured solids. They are soluble in methanol, acetone, acetonitrile and most of the organic solvents like benzene, DMF and DMSO but sparingly soluble in water.

FT-IR studies: The comparative study of FT-IR spectra of the complexes of dicarboxylic acid and diamines has been recorded and analyzed. The absence of -OH group of the carboxylic acid and free -NH_2 group of amino acids in the spectra confirms the formation of macrocyclic complexes. In the spectra the absorption band appeared at 3280-3252 cm^{-1}, corresponds to NH stretching vibration. Strong absorption band at 1630-1613 cm^{-1}, corresponds to the carbonyl group and medium intensity band appearing at 1581-1555 cm^{-1} confirmed the cyclization of product [39,40]. Medium intensity bands appeared in the region of ~2925-2810 cm^{-1} assigned due to

ν(C–H) of methyl group of complex [41]. The symmetric and asymmetric vibrations lies near ~ 1419-1400, ~ 1398-1370 cm^{-1}. The bands in the range of ~1277-1250 cm^{-1} corresponds to (N-H) of amide groups of the complexes. The C-N stretching [42] occurred within the range of ~1000-1340 cm^{-1}. Peaks in the region of ~480-412 cm^{-1} due to the ν(M-N) vibration [43,44] representing coordination to nitrogen (Fig. 1).

ESI-MS studies: In order to get the data regarding the monomeric or polymeric nature of the complexes, mass analysis was carried out. In nickel complex molecular ion peak $[M]^+$ is present at 680 *m/z* value that corresponds to $[M+2Na]^+$. In case of cobalt complex molecular ion peak is appeared at 633.13 *m/z* that corresponds to $[M+H]^+$. The mass spectrum of copper complex demonstrated the presence of molecular ion peak at 714.2 *m/z* that corresponds to $[M+2K]^+$. On the other hand, a small molecular ion peak at 737.22 *m/z* can be observed in the zoom spectra. Various peaks in spectra can be explained for various fragmentation patterns.

Thermogravimetric analysis: The thermogravimetric analysis of macrocyclic complexes has been carried out with N_2 flow of (20 mL/min) with the heating rate of 10 ºC/min at the range of 50-800 ºC. The thermal nature of the all the complexes has been recorded in the temperature range of 0-800 ºC. The TG curves of all the metal complexes are given in Fig. 2. The thermogram curve of $[Co(N_4Mac)Cl_2]$ is a four step breakdown with mass loss of 80%. There is no weight loss before 280 ºC, which implies that this complex is thermally stable upto 280 ºC. The first weight loss of 68% occurred in the temperature range of 280-340 ºC. The second weight loss of 2% occurred around temperature 349-376 ºC. Third weight loss of about 7% occurred at 381-531 ºC and fourth weight loss of 3% was found around 616-790 ºC. The thermogravimetric curve of nickel complex $[Ni(N_4Mac)Cl_2]$ exhibited thermal decomposition in four steps. TG curve imparts data that the first weight loss of 2% occurred around the temperature range of 51-108 ºC. Second breakdown between 141-266 ºC implies 22% weight loss. The third weight loss of 3% was discovered around 272-292 ºC. In the range of 300-785 ºC, the nickel complex displays a loss of 21%. Thermal analysis of copper complex $[Cu(N_4Mac)Cl_2]$ exhibited good thermal stability upto 229.89 ºC, which indicates the absence of coordi-nated water molecule in the complex sphere. The TG curve of copper complex shows a complete decomposition in 4 steps. The first weight loss of 14% was observed around 230-337 ºC. In the temperature range of 340-377 ºC, the complex loses 3% of its weight. The third breakdown has been recorded in between 380-456 ºC showing 14% weight loss. The fourth loss of 5% weight of the complex represents the thermal breakdown [45] in between the temperature range of 382-788 ºC. This data revealed that water molecules are neither present in the form of crystallization nor in the form of coordination.

Electron spin resonance spectral studies: The spectrum of copper tetraaza macrocyclic complex has been recorded on the X-band (frequency 8.75-9.65 GHz) at room temperature (Fig. 3). The magnetic field used for the analysis is 3,000 G and field center is 336.791 mT. The sweep time is 4.0 min. The spectrum of the copper macrocyclic complexes exhibited an anisotropic signal at room temperature and slightly hyperfine splitting is exhibited by the complexes at room temperature. Therefore, the value of $g_{\parallel}$ and $g_{\perp}$ were found to be 2.112

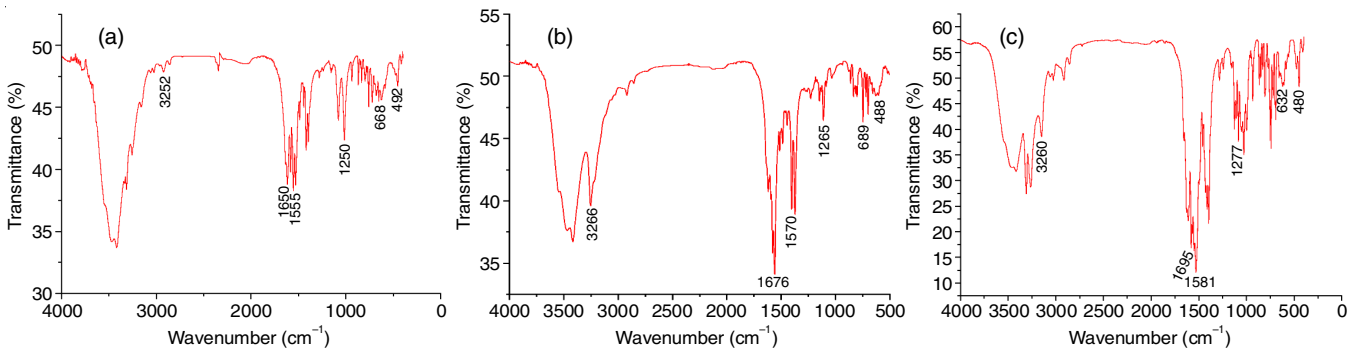

Fig. 1. IR spectrum of macrocyclic complexes of (a) DP1, (b) DP2 and (c) DP3

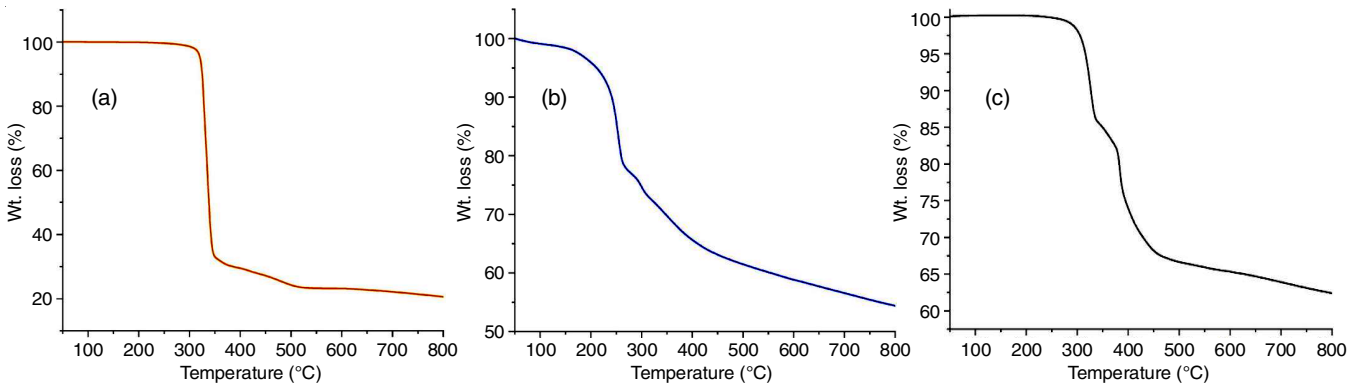

Fig. 2. Thermogravimetric analysis of macrocyclic complexes of (a) DP1, (b) DP2 and (c) DP3

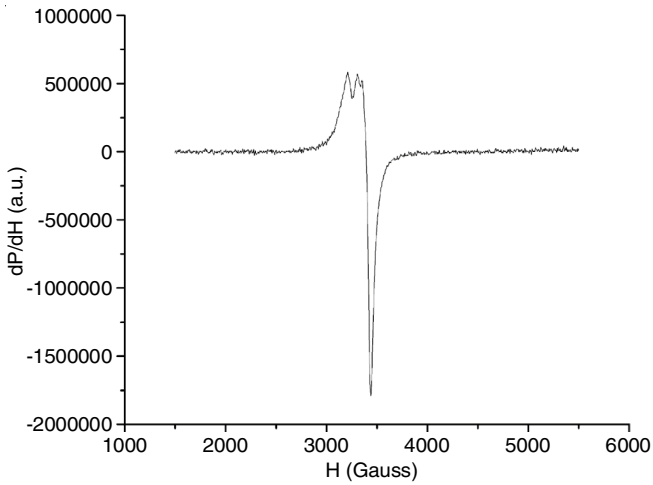

Fig. 3. EPR spectrum of copper macrocyclic complex (DP3)

and 2.098. The data revealed the octahedral geometry of Cu(II) macrocyclic complex and indicates the presence of an unpaired electron in d_{xy} orbital of the complexes [46].

Electronic spectral studies: The electronic spectra of the synthesized macrocyclic complexes were recorded in DMSO (Fig. 4). The magnetic moment of Co(II) complex at room temperature comes out 3.8 B.M. corresponds to three unpaired electrons. Electronic spectrum of cobalt complex exhibited bands at ~ 320-380 nm, ~ 270-290 nm and ~210-230 nm. These bands corresponds to the various transitions like ^4T_1g (F) → ^4T_2g (F), ^4T_1g (F) → ^4A_2g and ^4T_1g (F) → ^4A_2g (F). These transitions are in tune with that of octahedral geometry. The electronic spectrum of Ni(II) complex exhibited bands at ~550-560 nm, ~ 280-310 nm and ~230-255 nm transitions for ^3A_2g (F) → ^3T_2g (F), ^3A_2g (F) → ^3T_1g(F) and ^3A_2g (F) → ^3T_1g (P) transitions respectively. The observed magnetic moment at room temperature was 2.83 B.M. these values are comparable with that of the characteristic features of octahedral geometry. The ascertained magnetic moment for Cu(II) complex is 1.7 B.M. The electronic spectrum of Cu(II) macrocyclic complex exhibited bands at ~560-590 nm, ~280-295 nm and ~210-230 nm assigned for ^4T_1g (F) → ^4T_2g (F), ^4T_1g (F) → ^4A_2g and ^4T_1g (F) → T_1g (P), respectively are characteristic bands expected for octahedral geometry. These transitions of all the complexes are in good consistency with octahedral geometry [47].

Biological results

Antibacterial assay: The antimicrobial screening result after assessing the synthesized macrocyclic metal complexes against the selected microbes have been summarized in Table-1. The zone of inhibition of the bacterial growth of all the synthesized macrocyclic complexes has been investigated and then compared with that of the standard streptomycin [28]. All the tested macrocycles possess significant antibacterial activity against bacterial species. The results of the antibacterial activity displayed that cobalt macrocyclic complex exhibited best antibacterial efficacy against all bacterial species. This

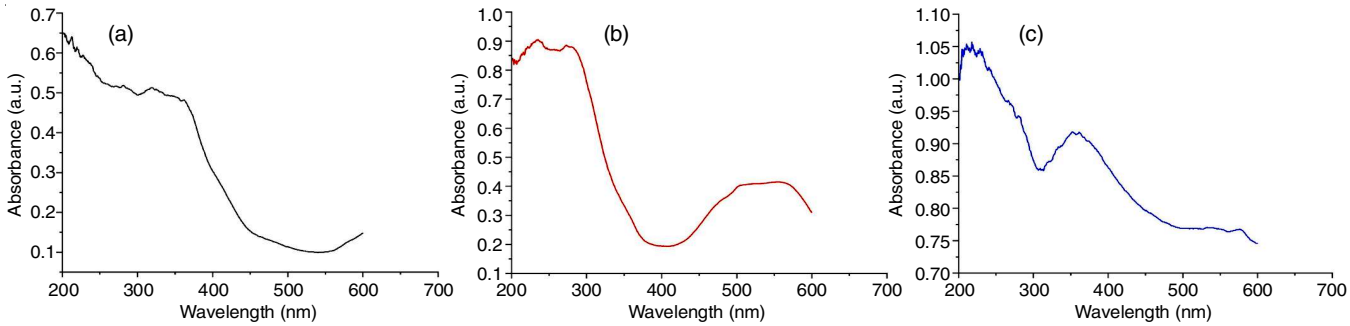

Fig. 4. UV-vis spectrum of macrocyclic complexes (a) DP1, (b) DP2 and (c) DP3

TABLE-1
ANTIBACTERIAL AND ANTIFUNGAL STUDIES OF MACROCYCLIC COMPLEXES of Co(II), Ni(II) AND Cu(II)

Test compound	Zone of inhibition (mm) at different concentration (mg/mL)					
	2.5	5.0	7.5	2.5	5.0	7.5
	Bacterial strain: *E. coli*			Bacterial strain: *P. aeruginosa*		
DP1	7.07 ± 0.12	8.23 ± 0.15	9.40 ± 0.17	6.23 ± 0.06	7.53 ± 0.10	8.63 ± 0.15
DP2	6.7 ± 0.15	7.5 ± 0.15	8.8 ± 0.20	5.97 ± 0.15	7.0 ± 0.31	8.23 ± 0.25
DP3	5.33 ± 0.26	6.37 ± 0.30	7.30 ± 0.32	5.01 ± 0.15	6.89 ± 0.12	8.21 ± 0.15
Streptomycin	21 ± 0.13	25 ± 0.18	25 ± 0.18	24 ± 0.0	28 ± 0.01	28 ± 0.02
	Bacterial strain: *B. subtilis*			Bacterial strain: *S. aureus*		
DP1	7.37 ± 0.10	8.57 ± 0.15	9.50 ± 0.25	6.70 ± 0.26	8.0 ± 0.15	9.10 ± 0.17
DP2	6.40 ± 0.20	7.63 ± 0.15	8.53 ± 0.10	5.77 ± 0.26	6.70 ± 0.10	7.90 ± 0.10
DP3	5.40 ± 0.15	7.07 ± 0.35	8.50 ± 0.30	5.50 ± 0.15	7.23 ± 0.26	7.80 ± 0.10
Streptomycin	12 ± 0.03	16 ± 0.01	18 ± 0.01	13 ± 0.02	18 ± 0.01	18 ± 0.11
	Fungal strain: *C. albicans*			Fungal strain: *A. niger*		
DP1	5.37 ± 0.06	6.67 ± 0.15	7.87 ± 0.25	6.35 ± 0.15	7.63 ± 0.20	9.00 ± 0.21
DP2	5.87 ± 0.21	7.03 ± 0.15	8.60 ± 0.20	6.17 ± 0.07	6.86 ± 0.15	8.86 ± 0.10
DP3	5.73 ± 0.15	7.27 ± 0.12	9.07 ± 0.15	4.93 ± 0.25	5.90 ± 0.21	7.67 ± 0.12
Itraconazole	11 ± 0.01	14 ± 0.02	15 ± 0.01	11 ± 0.06	13 ± 0.07	13 ± 0.10

TABLE-2
DETAILS ABOUT TARGET PROTEINS USED IN THE DOCKING STUDIES

PDB ID	Classification	Source organism	Expression system
3T88	Lyase/lyase inhibitor	*E. coli*	*E. coli* BL21 (DE3)
2W7Q	Protein transport	*P. aeruginosa*	–
5H67	DNA binding protein/cell cycle	*B. subtilis*	*E. coli* BL21 (DE3)
2DHN	Product complex	*S. aureus*	*Escherichia coli*
3DRA	Transferase	*C. albicans*	*Escherichia coli*
6IGY	Hydrolase	*A. niger*	*E. coli* BL21 (DE3)

can be explained on the basis of Tweedy's chelation theory, which disclosed that the polarity of the central metal ion decreases with chelation as the positive charge of the metal ion shares with the donor groups [48], which further enhances the lipophilic nature of the central metal ion of the macrocyclic complexes. This favours easy penetration through the lipid layer of cell membrane of the microorganism.

The results of *in vitro* antifungal activity of the synthesized complexes demonstrated that the complex of copper possess good antifungal activity against *C. albicans* whereas cobalt complex displayed excellent antifungal potential against *A. niger*.

Antioxidant activity: The DPPH scavenging activities of the macrocyclic complexes were expressed in IC_{50}, whose concentration is been adequate to obtain 50% of the maximum scavenging activity. The IC_{50} (μM) values of the macrocyclic complexes are displayed in Fig. 5. The result revealed that all macrocyclic complexes exhibited good antioxidant activity but cobalt complex (DP1) exhibited almost similar antioxidant activity as compared to than that of the standard ascorbic acid [49]. The order of the antioxidant activity of the macrocyclic complexes were in the order DP1 > DP2 > DP3 are accordant to their IC_{50} values in opposition to standard solution of ascorbic acid.

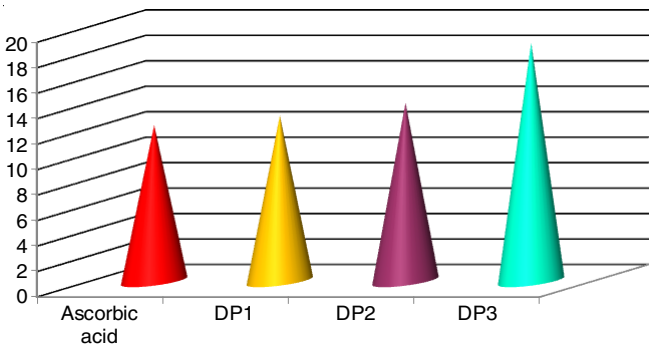

Fig. 5. Antioxidant activity of synthesized macrocyclic complexes

Molecular docking studies: The information related to the PDB IDs used in the current study is shown in Table-2 for instance the biological process for which these proteins are responsible from which organism these proteins are originally derived and the way in which proteins are synthesized, modified and regulated in the living organism. The backbone of ligands is substituted tetraamide macrocyclic ring interpolated with transition metals *viz.* cobalt, nickel and copper. The 2D and 3D structures of macrocyclic ligand (after optimization in Avogadro), while fully optimized structures of Co(II), Ni(II) and Cu(II) complexes obtained from Avogadro software are shown in Fig. 6.

Bond angles of the central metal atoms with adjacent six atoms (four nitrogen atoms from the macrocyclic ring and two atoms of chloride) are shown in Table-3, which indicates octahedral structure in all complexes.

TABLE-3
SELECTED BOND ANGLES OF COBALT, NICKEL AND COPPER COMPLEXES

DP1		DP2		DP3	
Atom connectivity	Bond angle (°)	Atom connectivity	Bond angle (°)	Atom connectivity	Bond angle (°)
Cl-Co-N	88.2	Cl-Ni-N	88.3	Cl-Cu-N	86.8
Cl-Co-N	86.8	Cl-Ni-N	92.6	Cl-Cu-N	92.4
Cl-Co-N	92.0	Cl-Ni-N	91.8	Cl-Cu-N	89.1
Cl-Co-N	93.0	Cl-Ni-N	87.2	Cl-Cu-N	89.5
Cl-Co-N	86.9	Cl-Ni-N	91.8	Cl-Cu-N	86.9
Cl-Co-N	87.9	Cl-Ni-N	92.9	Cl-Cu-N	90.8
Cl-Co-N	93.2	Cl-Ni-N	88.1	Cl-Cu-N	91.3
Cl-Co-N	91.9	Cl-Ni-N	87.3	Cl-Cu-N	93.3
Cl-Co-Cl	179.9	Cl-Ni-Cl	179.9	Cl-Cu-Cl	179.2

The negative and low binding affinity values indicated strong bonds between proteins and ligands that demonstrated favourable conformation of proteins. The energy for 3DRA (-11.8 kcal/mol) was found to be lower than the other proteins: 3T88 with -9.8 kcal/mol, 5H67 with -10.3 kcal/mol, 2DHN with -9.5 kcal/mol, 6IGY with -10.7 kcal/mol and 2W7Q with -9.1 kcal/mol, stating that DP1 complex has better binding affinity than others in this analysis (Table-4). The molecular binding assessment showed the large involvement of interaction forces between the DP1 and 2DHN with one hydrogen bond (Table-5) and strong hydrophobic interactions. DP1 formed a hydrogen bond with LYS8B; pi-sigma interaction with MET10A; pi-pi hydrophobic interactions with PHE58A and TYR54A; pi-alkyl hydrophobic interactions with TYR54A, PHE58A and LYS8A as shown in Fig. 7. DP2 (-9.0 kcal/mol) and DP3 (-8.9 kcal/mol) also unveiled a good binding score.

TABLE-4
BINDING AFFINITIES (kcal/mol) OF ALL LIGANDS WITH DIFFERENT PROTEINS

PDB ID	Binding affinity (kcal/mol)		
	DP1	DP2	DP3
2DHN	-9.5	-9.0	-8.9
3T88	-9.8	-9.3	-9.2
5H67	-10.3	-10.1	-10.0
2W7Q	-9.1	-9.1	-9.1
3DRA	-11.5	-11.7	-11.8
6IGY	-10.7	-10.7	-10.6

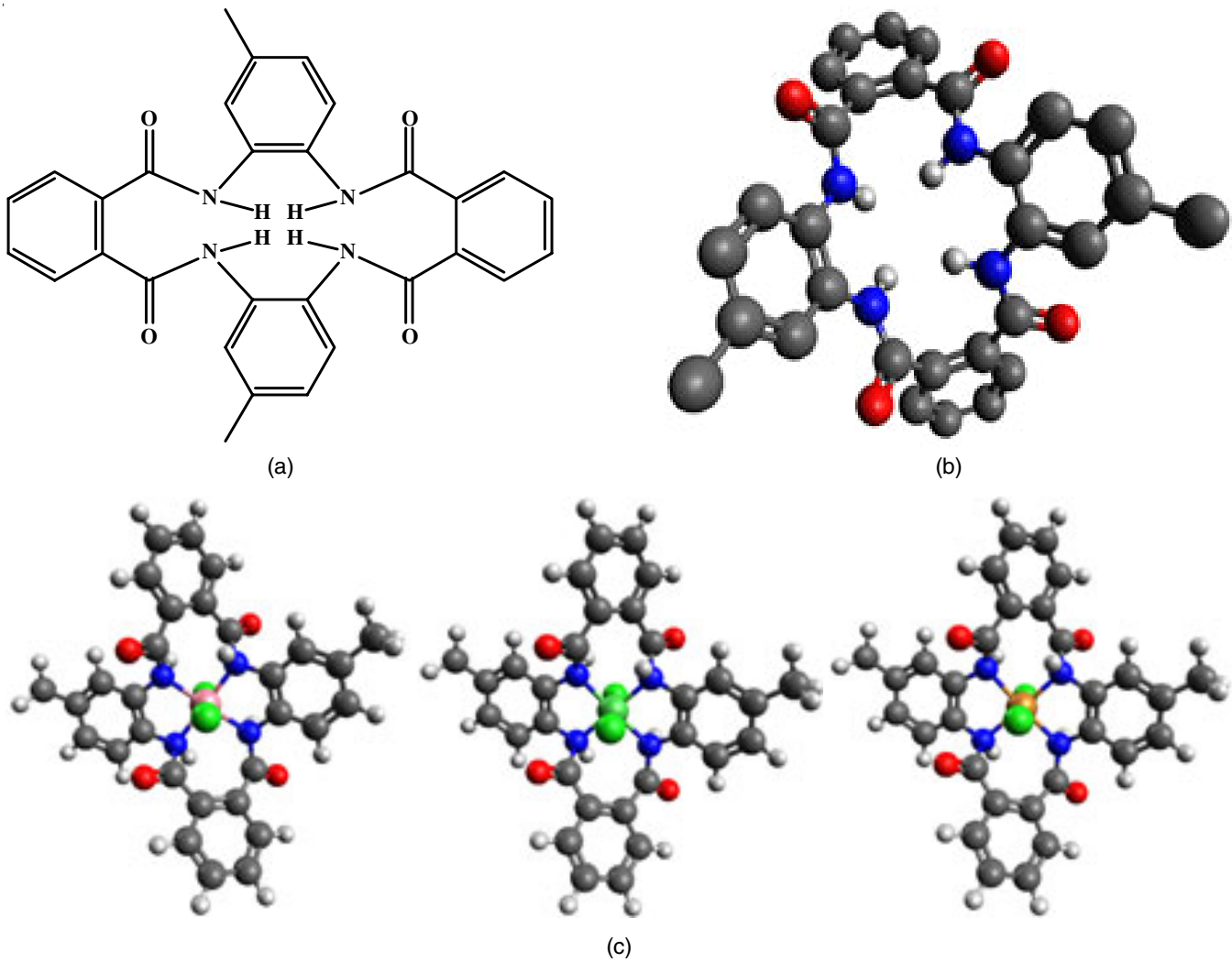

Fig. 6. Diagramatic representation of macrocyclic ligands (a) 2D structure (b) 3D Ball and Stick model of ligand (c) Optimized structures of cobalt, nickel and copper complexes; colour representation: red for oxygen, blue for nitrogen, green for chlorine (above and below the plane), pink for cobalt, green (in the plane) for nickel and golden for copper

TABLE-5
AMINO ACID RESIDUES OF THE TARGET PROTEIN ARE COMPREHENDED IN INTERACTION WITH THE BEST-SCORING MACROCYCLIC LIGAND

Ligand receptor	Ligand	Binding affinity (Kcal/mol)	Amino acids involved in interactions	H-Bonds formed
2DHN	DP1	-9.5	LYS8A, MET10A, PHE58A, TYR54A	1
3T88	DP1	-9.8	ARG173B, GLY242B, GLN243D, LEU246D	0
5H67	DP1	-10.3	ARG45A, SER52A, ARG54A, SER55A, LYS135A, LYS145A	4
2W7Q	DP1	-9.1	GLN171A, GLN53A, MET165A	3
3DRA	DP3	-11.8	ASN30B, ARG160B, SER65A, TYR103A, TYR67A, HIS145A, MET348B, GRG1721B	3
6IGY	DP1	-10.7	TRP109A, TYR150A, LYS196A, ASP218A, TYR219	2

Hydrogen bonds formed between the compound and the protein usually contribute to the stability of protein-ligand complexes; a large number of hydrogen bonds form more stable complexes [50].

The target protein 3T88 set forth electrostatic and hydrophobic interactions with DP1 resulting in better binding affinity (-9.8 kcal/mol) than DP2 (-9.3 kcal/mol) and DP3 (-9.2 kcal/mol). The interactions displayed were pi-cation electrostatic interactions with ARG173B; Amide-pi-stacked hydrophobic interaction with GLY242B and GLN243D where amide of the amino group and pi-orbitals of ligand were involved. Alkyl-alkyl hydrophobic interaction with LEU246D is shown in Fig. 8.

The molecular docking study of 5H67 protein with all these ligands revealed that DP1 showed minimum binding energy (-10.3 kcal/mol) in contrast with others: DP2 (-10.1 kcal/mol) and DP3 (-10.0 kcal/mol). DP1 interacted with the target protein through four hydrogen bonds with SER52A,

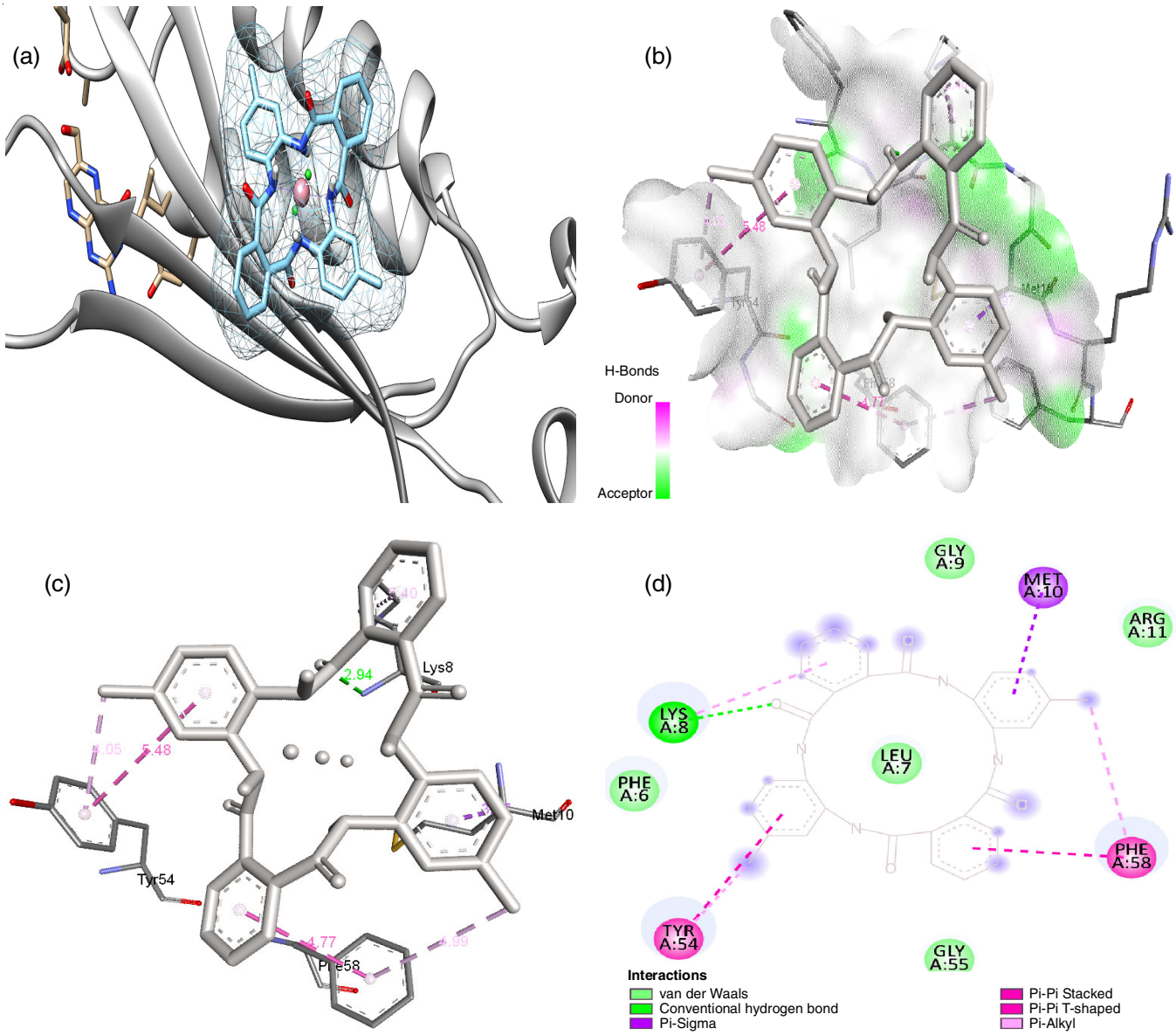

Fig. 7. (a) The best-predicted ligand docking pose for 2DHN is superposed with the DP1 ligand (b) Hydrogen bond donor (pink colour) and acceptor regions (green colour) of protein shaded by colours accordingly. (c) The nonbonding interaction between protein and ligand is green for hydrogen bonding and pink for hydrophobic interactions. (d) The pocket amino acid residues and amino acid residues involved in non-bonding interactions are represented in 2D format

SER55A and LYS145A; pi-cation electrostatic interaction with ARG45A, ARG54A and LYS145A; pi-alkyl hydrophobic interactions with LYS135A, LYS145A, ARG54A (Fig. 9).

In case of molecular docking with 2W7Q, the binding score for other ligands was similar to DP1 as -9.1 kcal/mol. DP1 interacted through two conventional hydrogen bonds with GLN171A and GLN53A (Table-6) and pi-donor hydrogen bond with GLN53A; pi-sulpfur interaction with MET165A (Table-5). The pocket amino acid residues for the DP1 are MET165A, THR106A, LEU147A, THR44A, GLN171A, ARG51A, GLN53A, ASN75A, THR55A, THR71A, TRP69A, GLN42A, THR108A, ARG104A and GLN107A (Fig. 10).

DP3 was found to be the most suitable ligand in terms of binding affinity towards the target protein 3DRA. DP3 showed one hydrogen bond with each: ASN30B, ARG160B, SER65A (Table-6) accompanied by pi-pi stacked hydrophobic interactions with TYR103A, pi-pi T-shaped hydrophobic interaction with TYR103A, pi-alkyl hydrophobic interactions with TYR67A, TYR103A, HIS145A, MET348B, GRG1721B (Table-5). The other amino acid residues lying in the binding groove were TRP300B, PHE37B, SER95B, ASN93B, SER65A and GLN104A. DP2 and DP1 also revealed good interactions with protein leading to the remarkable binding energy value of -11.7 and -11.5 kcal/mol respectively. All these interactions of 3DRA protein with DP3 ligand are shown in Fig. 11.

The ligand DP1 interacted with the protein 6IGY through hydrogen bonding, electrostatic and hydrophobic interactions revealing the binding affinity-10.7 kcal/mol. The non-bonding interactions involved were: hydrogen bond with TYR150A, LYS196A where ligand was hydrogen acceptor; pi-anion electro-

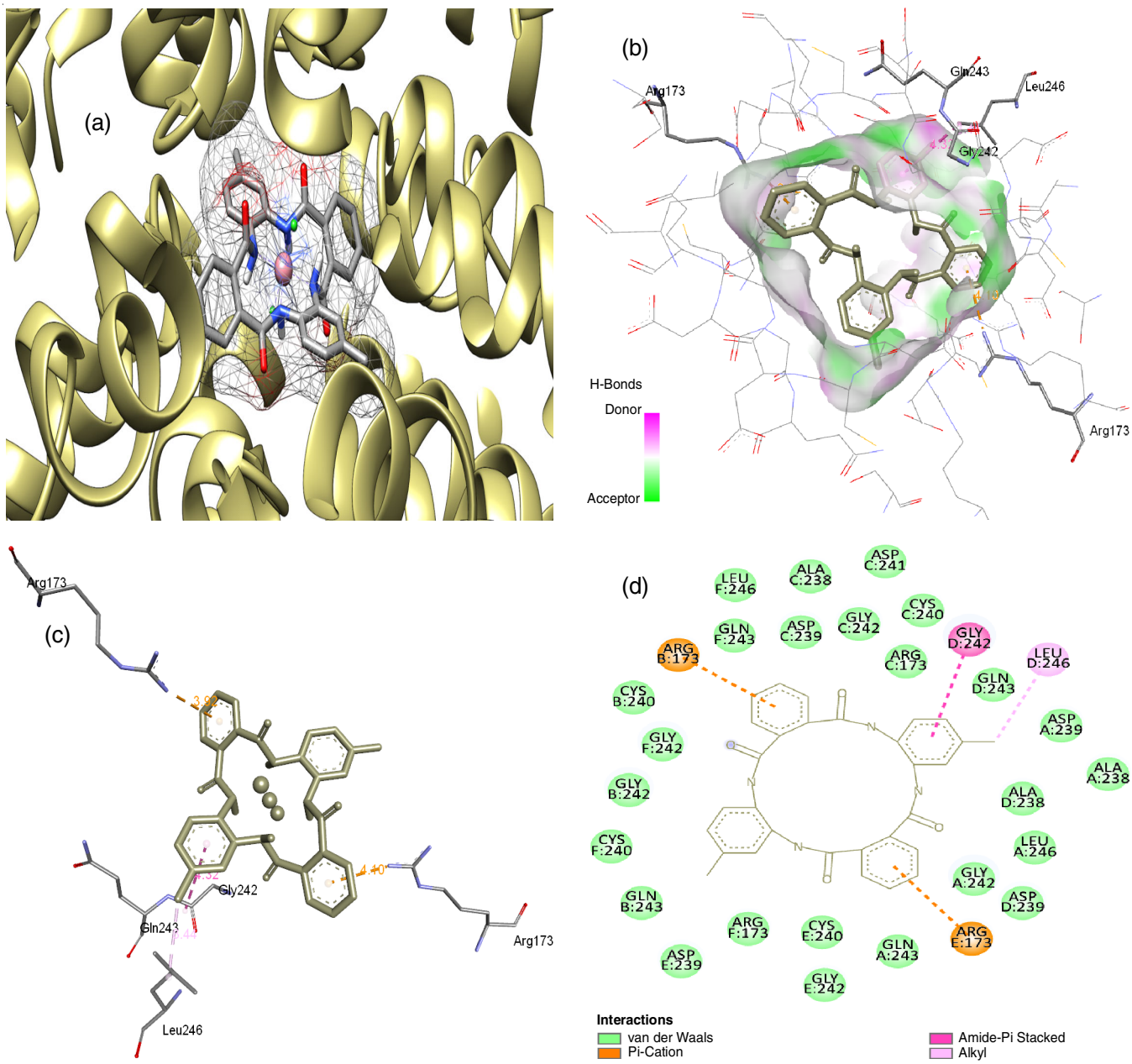

Fig. 8. (a) The best-predicted ligand docking pose for 3T88 is superposed with the DP1 ligand (b) Hydrogen bond donor (pink colour) and acceptor regions (green colour) of protein shaded by colours accordingly (c) The nonbonding interaction between protein and ligand is green for hydrogen bonding and pink for hydrophobic interactions (d) The pocket amino acid residues and amino acid residues involved in non-bonding interactions are represented in 2-D format

TABLE-6
STUDY OF HYDROGEN BOND INTERACTIONS BETWEEN LIGANDS HAVING THE BEST DOCKING ENERGY AND AMINO ACID RESIDUES OF PROTEINS

Protein with ligand	Donor atom	Acceptor atom	Distance (Å)	Protein with ligand	Donor atom	Acceptor atom	Distance (Å)
2DHN with DP1	ARG273B	O of ligand	2.94328	2W7Q with DP1	H from ligand	GLN171A	2.84144
	ARG273B	O of ligand	3.32756		H from ligand	GLN53A	2.43397
	TYR515B	O of ligand	3.21845		GLN53A	Pi-orbitals of ligand	3.42528
5H67 with DP1	SER52A	O of ligand	3.14223	3DRA with DP3	ASN30B	O of ligand	3.09484
	SER55A	O of ligand	3.01797		ARG160B	O of ligand	2.87059
	LYS145A	O of ligand	3.00781		SER65A	O of ligand	3.72665
	LYS145A	Pi-Orbitals	3.53698	6IGY with DP1	TYR150A	O of ligand	2.93572
					LYS196A	O of ligand	3.04140

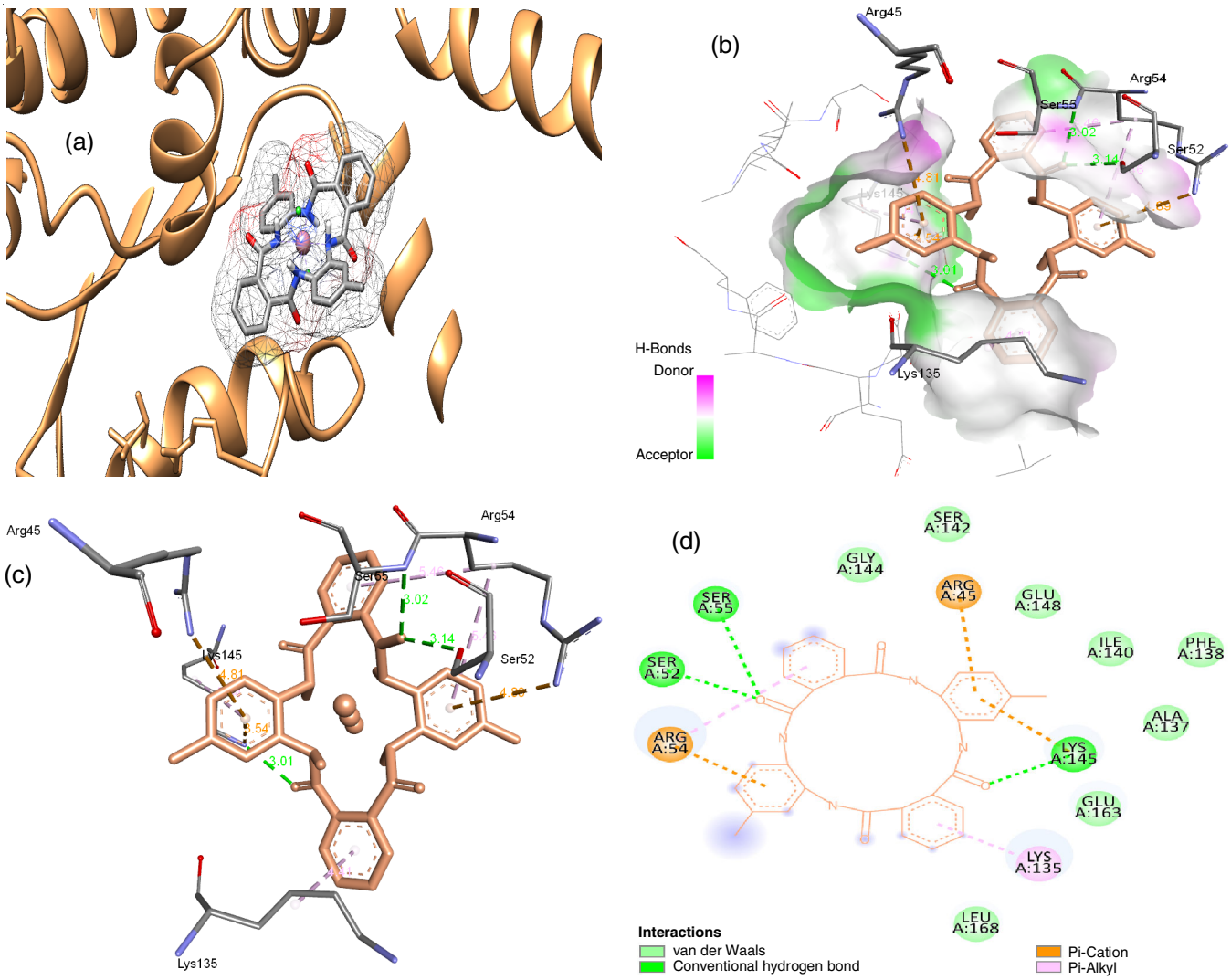

Fig. 9. (a) The best-predicted ligand docking pose for 5H67 is superposed with the DP1 ligand (b) Hydrogen bond donor (pink colour) and acceptor regions (green colour) of protein shaded by colours accordingly. (c) The nonbonding interaction between protein and ligand is green for hydrogen bonding and pink for hydrophobic interactions. (d) The pocket amino acid residues and amino acid residues involved in nonbonding interactions are represented in 2-D format

static interaction with ASP218A; pi-pi stacked hydrophobic interaction with TRP109A and pi-alkyl hydrophobic interaction with TYR219. The binding pocket was constituted with TRP109A, TYR111A, TYR150A, LYS196A, TYR217A, ASP218A, TYR219A, TRP223A and PHE245A amino acid residues (Fig. 12).

Conclusion

In this work, the synthesis of phthalic acid based transition metal coordinated macrocyclic complexes were conducted and characterized by ESR, IR, mass, electronic spectra, TGA and conductivity measurements studies. The studies revealed an octahedral geometry for all the synthesized complexes. There was a correlation between the presence of metal ions in the coordination sphere of the synthesized macrocyclic complexes and their antibacterial and antioxidant activities, suggesting that the presence of metal ions contributed to the enhanced biological activity. All the synthesized metal complexes impart substantial DPPH scavenging activity and the data revealed their good antioxidant nature. The experimental results against microbes were verified by molecular docking results. The molecular docking investigations unveil the momentous biological potency of cobalt macrocyclic complexes (DP1) against all the microbes in comparison to nickel (DP2) and copper (DP3) complexes.

CONFLICT OF INTEREST

The authors declare that there is no conflict of interests regarding the publication of this article.

REFERENCES

1. H. Keypour, N. Ansari, M. Mahmoudabadi, R. Karamian, S.H.M. Farida, M.E. Moghadam and R.W. Gable, *Inorg. Chim. Acta*, **509**, 119705 (2020); https://doi.org/10.1016/j.ica.2020.119705
2. R. Kanaoujiya, D. Kumar Sahu, V. Shankar, Garima and S. Srivastava, *Mater. Today Proc.*, **62**, 3497 (2022); https://doi.org/10.1016/j.matpr.2022.04.303
3. M.M. Keypour, F. Forouzandeh, R. Azadbakht, J. Khanabadi and M.A. Moghadam, *J. Mol. Struct.*, **1232**, 130024 (2021); https://doi.org/10.1016/j.molstruc.2021.130024

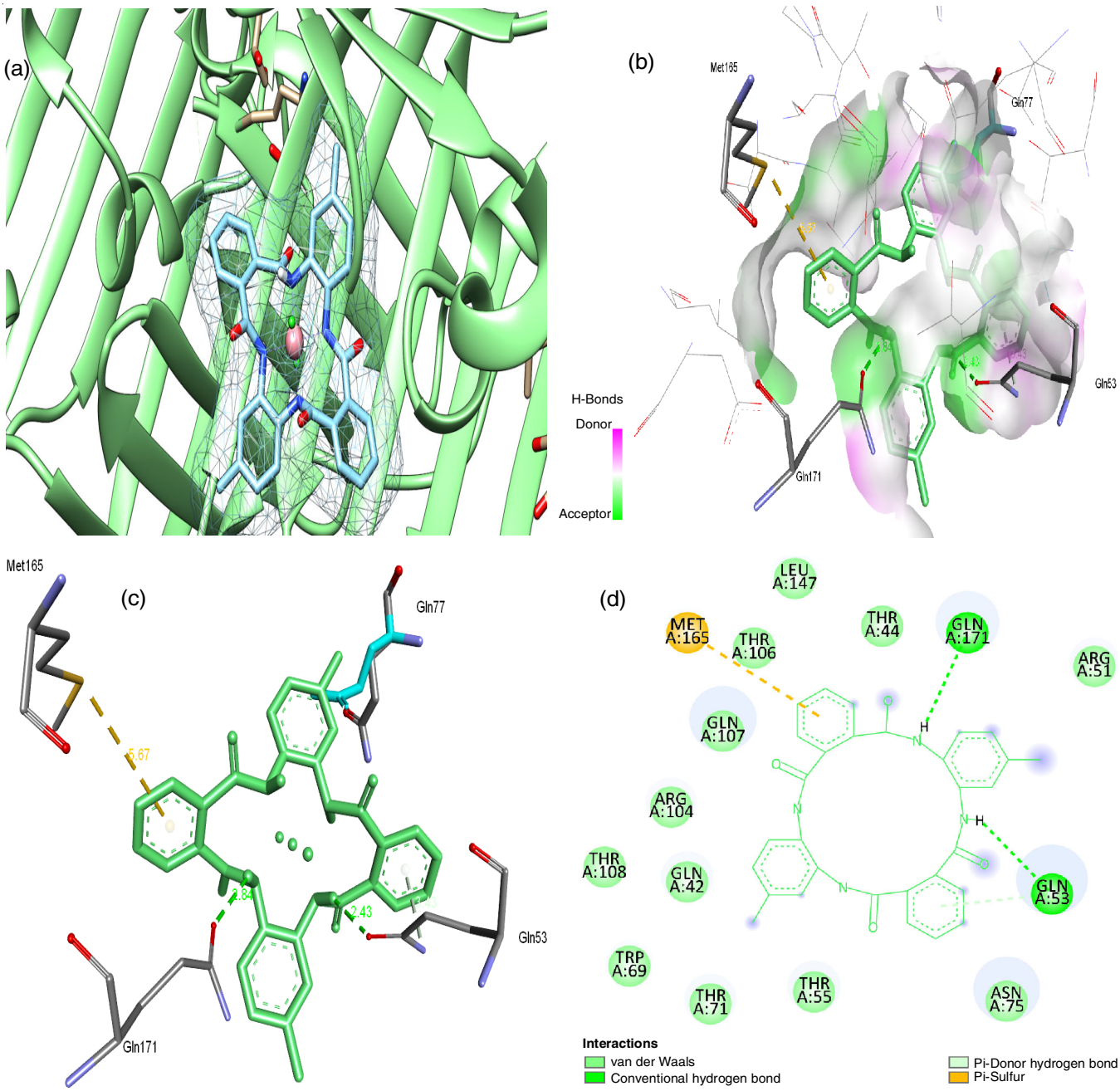

Fig. 10. (a) The best-predicted ligand docking pose for 2W7Q is superposed with the DP1 ligand (b) Hydrogen bond donor (pink colour) and acceptor regions (green colour) of protein shaded by colours accordingly. (c) The nonbonding interaction between protein and ligand is green for hydrogen bonding and pink for hydrophobic interactions. (d) The pocket amino acid residues and amino acid residues involved in nonbonding interactions are represented in 2D format

4. Y.L. Li, N. Wang, H.T. Lei, X.L. Li, H.Q. Zheng, H.Y. Wang, W. Zhang and R. Cao, *Coord. Chem. Rev.*, **442**, 213996 (2021); https://doi.org/10.1016/j.ccr.2021.213996
5. R. Kanaoujiya, D. Singh, T. Minocha, S.K. Yadav and S. Srivastava, *Mater. Today Proc.*, **65**, 3143 (2022); https://doi.org/10.1016/j.matpr.2022.05.354
6. N. Fahmi, I. Masih and K. Soni, *J. Macromol. Sci. A Pure Appl. Chem.*, **52**, 548 (2015); https://doi.org/10.1080/10601325.2015.1039334
7. M. Krstic, B. Petkovi, M. Mil, D. Mi and J.F. Santibanez, *Macedonian Chem. Chem Eng.*, **38**, 1 (2019); https://doi.org/10.20450/mjcce.2019.1599
8. A.J. Schuman, A. Raghavan, S.D. Banziger, Y. Song, Z.-B. Hu, B.L. Mash, A.L. Williams and T. Ren, *Inorg. Chem.*, **60**, 4447 (2021); https://doi.org/10.1021/acs.inorgchem.0c03224
9. C.J.M. Brown and R.J. Codd, *J. Inorg. Biochem.*, **216**, 111337 (2021); https://doi.org/10.1016/j.jinorgbio.2020.111337
10. T. Joshi, B. Graham and L. Spiccia, *Acc. Chem. Res.*, **48**, 2366 (2015); https://doi.org/10.1021/acs.accounts.5b00142
11. M.O.F. Khan, J. Keiser, P.N.A. Amoyaw, M.F. Hossain, M. Vargas, J.G. Le, N.C. Simpson, K.D. Roewe, T.R.N.C. Freeman, T.R. Hasley, R.D. Maples, S.J. Archibald and T.J. Hubin, *Antimicrob. Agents Chemother.*, **60**, 5331 (2016); https://doi.org/10.1128/AAC.00778-16
12. T.J. Hubin, A.N. Walker, D.J. Davilla, T.R.N. Carder Freeman, B.M. Epley, T.R. Hasley, P.N.A. Amoyaw, S. Jain, S.J. Archibald, T.J. Prior, J.A. Krause, A.G. Oliver, B.L. Tekwani and M.O.F. Khan, *Polyhedron*, **163**, 42 (2019); https://doi.org/10.1016/j.poly.2019.02.027

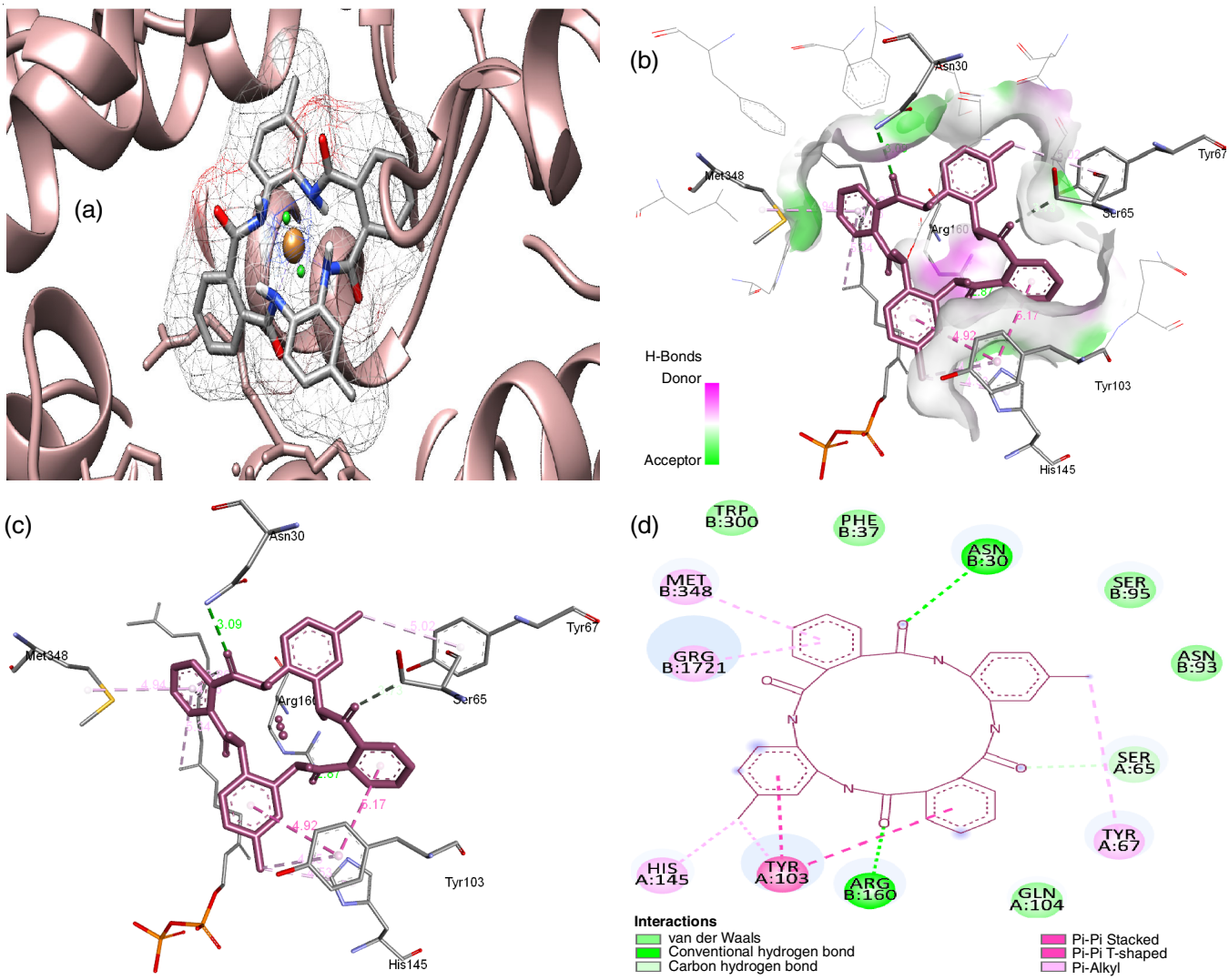

Fig. 11. (a) The best-predicted ligand docking pose for 3DRA is superposed with the DP3 ligand (b) Hydrogen bond donor (pink colour) and acceptor regions (green colour) of protein shaded by colours accordingly (c) The nonbonding interaction between protein and ligand is green for hydrogen bonding and pink for hydrophobic interactions (d) The pocket amino acid residues and amino acid residues involved in nonbonding interactions are represented in 2D format

13. H. Zafar, A. Kareem, A. Sherwani, O. Mohammad, M.A. Ansari, H.M. Khan and T.A. Khan, *J. Photochem. Photobiol. B*, **142**, 8 (2015); https://doi.org/10.1016/j.jphotobiol.2014.10.004
14. A. Kareem, H. Zafar, A. Sherwani, O. Mohammad and T.A. Khan, *J. Mol. Struct.*, **1075**, 17 (2014); https://doi.org/10.1016/j.molstruc.2014.06.073
15. E.J.P. Malar, R. Jacob and S. Balasubramanian, *J. Chem. Sci.*, **131**, 110 (2019); https://doi.org/10.1007/s12039-019-1688-4
16. M. Asadi, H. Sepehrpour and K. Mohammadi, *J. Serb. Chem. Soc.*, **76**, 63 (2011); https://doi.org/10.2298/JSC100104004A
17. P. Gull, M.A. Malik, O.A. Dar and A.A. Hashmi, *J. Mol. Struct.*, **1134**, 734 (2017); https://doi.org/10.1016/j.molstruc.2017.01.033
18. J. Li, R. Liu J. Jiang, X. Liang, G. Huang, D. Yang, H. Chen, L. Pan and Z. Ma, *J. Inorg. Biochem.*, **210**, 111165 (2020); https://doi.org/10.1016/j.jinorgbio.2020.111165
19. S. Chandra and Ruchi, *Spectrochim. Acta A Mol. Biomol. Spectrosc.*, **103**, 338 (2013); https://doi.org/10.1016/j.saa.2012.10.065
20. M.A. Nikolic, K.M. Szécsényi, B. Dra•ic, M.V. Rodic, V. Stanic and S. Tanaskovic, *J. Mol. Struct.*, **1236**, 130133 (2021); https://doi.org/10.1016/j.molstruc.2021.130133
21. P. Rajakkani, A. Alagarraj and S.A.G. Thangavelu, *Inorg. Chem. Commun.*, **134**, 108989 (2021); https://doi.org/10.1016/j.inoche.2021.108989
22. L. Mandal, S. Majumder and S. Mohanta, *Dalton Trans.*, **45**, 17365 (2016); https://doi.org/10.1039/C6DT02631A
23. S. Das, J. Adhikary, P. Chakraborty, T. Chakraborty and D. Das, *RSC Adv.*, **6**, 98620 (2016); https://doi.org/10.1039/C6RA05478A
24. T. Chakraborty, S. Mukherjee, R. Parveen, A. Chandra, D. Samanta and D. Das, *New J. Chem.*, **45**, 2550 (2021); https://doi.org/10.1039/D0NJ05635A
25. S. Ullmann, R. Schnorr, M. Handke, C. Laube, B. Abel, J. Matysik, M. Findeisen, R. Rüger, T. Heine and B. Kersting, *Chem. Eur. J.*, **23**, 3824 (2017); https://doi.org/10.1002/chem.201700253
26. M. Upadhyay, R.V. Singh and N. Fahmi, *Res. J. Chem. Sci.*, **12**, 18 (2022).
27. A. Pilon, J. Lorenzo, S. Rodriguez-Calado, P. Adao, A.M. Martins, A. Valente and L. Alves, *ChemMedChem*, **14**, 770 (2019); https://doi.org/10.1002/cmdc.201800702
28. N. Fahmi, M. Upadhyay, N. Sharma and S. Belwal, *J. Chem. Res.*, **44**, 336 (2020); https://doi.org/10.1177/1747519819893885
29. N. Ghaffar, S. Javad, M.A. Farrukh, A.A. Shah, M.K. Gatasheh, B.M.A. Al-Munqedhi and O. Chaudhry, *PLoS One*, **17**, e0264588 (2022); https://doi.org/10.1371/journal.pone.0264588

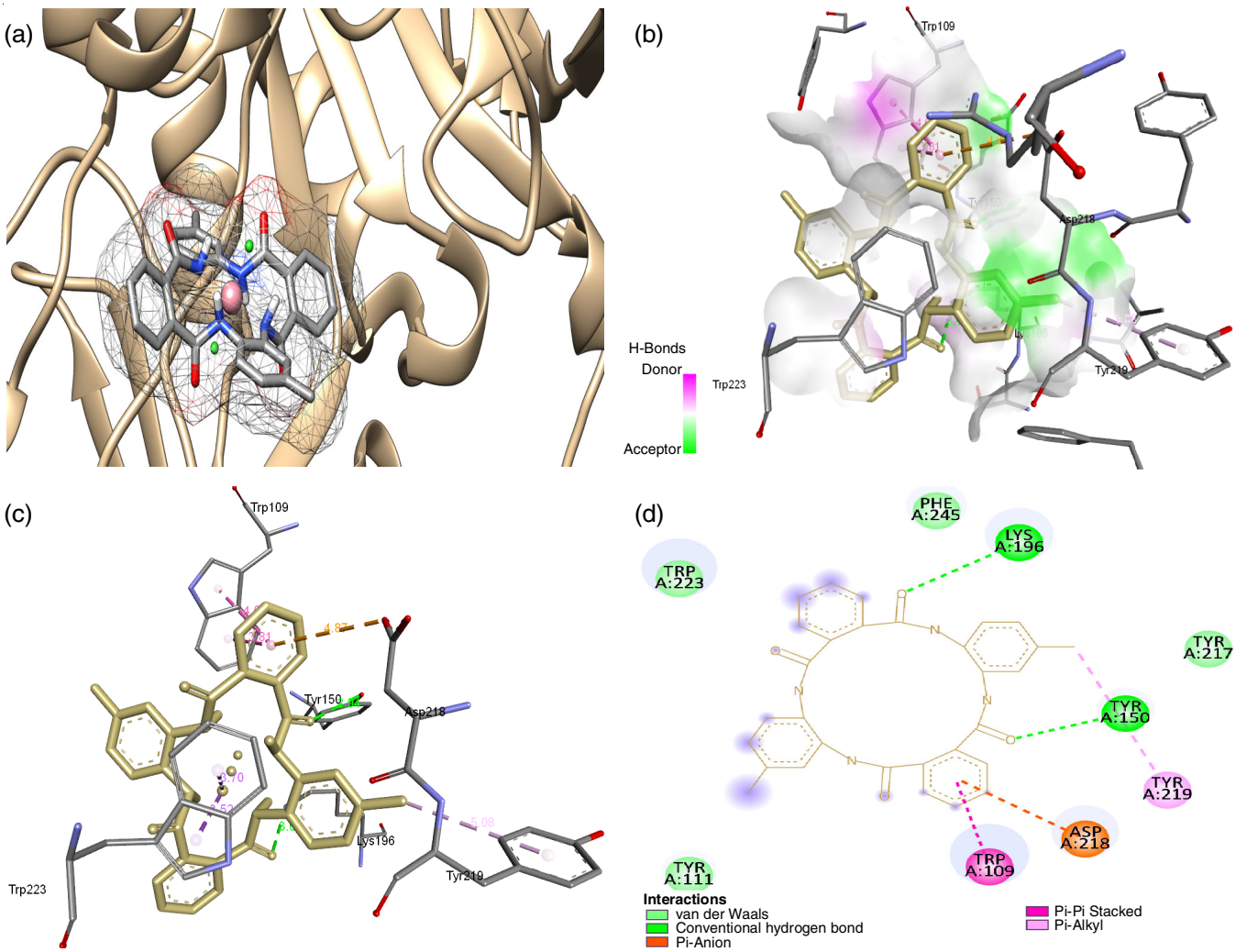

Fig. 12. (a) The best-predicted ligand docking pose for 6IGY is superposed with the DP1 ligand (b) Hydrogen bond donor (pink colour) and acceptor regions (green colour) of protein shaded by colours accordingly (c) The nonbonding interaction between protein and ligand is green for hydrogen bonding and pink for hydrophobic interactions (d) The pocket amino acid residues and amino acid residues involved in nonbonding interactions are represented in 2-D format

30. Z. You, X. Ran, Y. Dai and Y.J. Ran, *J. Mycol. Med.*, **28**, 492 (2018); https://doi.org/10.1016/j.mycmed.2018.03.007
31. S. Lamba, M. Agrawal and S. Bugalia, *Int. J. Sci. Res.*, **6**, 1488 (2013).
32. P. Molyneux, *Songklanakarin J. Sci. Technol.*, **26**, 211 (2004).
33. M.D. Hanwell, D.E. Curtis, D. Lonie, C.T. Vandermeersch, E. Zurek and G.R.J. Hutchison, *J. Cheminform.*, **4**, 17 (2012); https://doi.org/10.1186/1758-2946-4-17
34. H.D. Snyder and T.G. Kucukkal, *J. Chem. Educ.*, **98**, 1335 (2021); https://doi.org/10.1021/acs.jchemed.0c00959
35. S. Forli, R. Huey, M.E. Pique, M.F. Sanner, D.S. Goodsell and A.J. Olson, *Nat. Protoc.*, **11**, 905 (2016); https://doi.org/10.1038/nprot.2016.051
36. O. Trott and A.J. Olson, *J. Comput. Chem.*, **31**, 455 (2010); https://doi.org/10.1002/jcc.21334
37. D. Salha, M. Andaç and A. Denizli, *J. Mol. Recognit.*, **34**, E2875 (2021); https://doi.org/10.1002/jmr.2875
38. E.F. Pettersen, T.D. Goddard, C.C. Huang, G.S. Couch, D.M. Greenblatt, E.C. Meng and T.E. Ferrin, *J. Comput. Chem.*, **25**, 1605 (2004); https://doi.org/10.1002/jcc.20084
39. S. Chauhan, M. Swami, S. Malik and R.V. Singh, *Main Group Met. Chem.*, **31**, 263 (2008); https://doi.org/10.1515/MGMC.2008.31.5.263
40. M.H. Abo-Ghalia, G.O. Moustafa, A.E.G.E. Amr, A.M. Naglah, E.A. Elsayed and A.H. Bakheit, *Molecules*, **25**, 1253 (2020); https://doi.org/10.3390/molecules25051253
41. I. Masih, N. Fahmi and Rajkumar, *J. Enzyme Inhib. Med. Chem.*, **28**, 33 (2013); https://doi.org/10.3109/14756366.2011.625022
42. O.H.S. Al-Obaidi and A.R. Al-Hiti, *Am. Chem. Sci. J.*, **2**, 1 (2012); https://doi.org/10.9734/ACSJ/2012/1063
43. S.K. Das Gupta, S. Rabi, D. Ghosh, F. Yasmin, B.K. Dey, S. Dey and T.G. Roy, *J. Chem. Sci.*, **133**, 7 (2021); https://doi.org/10.1007/s12039-020-01861-7
44. V. Sangwan and D.P. Singh, *Mater. Sci. Eng. C*, **105**, 110119 (2019); https://doi.org/10.1016/j.msec.2019.110119
45. J.H. Pandya, M. Travadi, R.N. Jadeja, R.N. Patel and V.K. Gupta, *J. Indian Chem. Soc.*, **99**, 100403 (2022); https://doi.org/10.1016/j.jics.2022.100403
46. K. Sharma, D.P. Singh and V. Kumar, *Indian J. Chem. Technol.*, **24**, 534 (2017).
47. M. Tyagi, S. Chandra and P. Tyagi, *Spectrochim. Acta A Mol. Biomol. Spectrosc.*, **117**, 1 (2014); https://doi.org/10.1016/j.saa.2013.07.074
48. A. Singh and A. Chaudhary, *Bioinorg. Chem. Appl.*, **2018**, 2467463 (2018); https://doi.org/10.1155/2018/2467463
49. O.P. Sharma and T.K. Bhat, *Food Chem.*, **113**, 1202 (2009); https://doi.org/10.1016/j.foodchem.2008.08.008
50. C.G.P. Doss and N. Nagasundaram, *PLoS One*, **7**, e31677 (2012); https://doi.org/10.1371/journal.pone.0031677